

Article

The Influence of Viscosity on Heat Dissipation under Conditions of the High-Frequency Oscillating Magnetic Field

Matus Molcan ^{1,*}, Andrzej Skumiel ², Jana Tothova ³, Katarina Paulovicova ¹, Peter Kopcansky ¹
and Milan Timko ¹

¹ Institute of Experimental Physics, Slovak Academy of Sciences, Watsonova 47, 04001 Kosice, Slovakia; paulovic@saske.sk (K.P.); kopcan@saske.sk (P.K.); timko@saske.sk (M.T.)

² Faculty of Physics, Adam Mickiewicz University, Uniwersytetu Poznańskiego 2, 61-614 Poznań, Poland; andrzej.skumiel@amu.edu.pl

³ Department of Physics, Faculty of Electrical Engineering and Informatics, Technical University of Kosice, Park Komenskeho 2, 04200 Kosice, Slovakia; jana.tothova@tuke.sk

* Correspondence: molcan@saske.sk

Abstract: High-frequency components such as microprocessors, transistors, antennas, voltage-controlled oscillators, and many others generate a large amount of heat. In the absence of satisfactory cooling, these components may suffer damage or even destruction. Therefore, it is important to find effective ways to cool these components. A possible solution is to use oil-based magnetic fluids. Magnetic fluids contain magnetic particles dispersed in oil, and their properties, including viscosity, affect their cooling capabilities. Viscosity can be changed by adding various additives or by adjusting the concentration of magnetic particles. The advantage of using oil-based magnetic fluids for cooling is that they allow for precise dosing and control of the amount of fluid applied to the component, reducing thermal losses and increasing cooling efficiency. In addition, oil-based magnetic fluids can also act as a dielectric, reducing electrical noise and increasing electromagnetic compatibility with the components. Analyzing the heating rate of magnetic fluids consisting of mineral oils in an alternating magnetic field with a frequency of 500 kHz, we have shown the capability of controlling thermal losses by adjusting the viscosity of the carrier liquid.

Keywords: magnetic fluid; viscosity; oscillating magnetic field; heating; shear rate



Citation: Molcan, M.; Skumiel, A.; Tothova, J.; Paulovicova, K.; Kopcansky, P.; Timko, M. The Influence of Viscosity on Heat Dissipation under Conditions of the High-Frequency Oscillating Magnetic Field. *Magnetochemistry* **2024**, *10*, 2. <https://doi.org/10.3390/magnetochemistry10010002>

Academic Editor: Xuegeng Yang

Received: 27 November 2023

Revised: 13 December 2023

Accepted: 21 December 2023

Published: 24 December 2023



Copyright: © 2023 by the authors. Licensee MDPI, Basel, Switzerland. This article is an open access article distributed under the terms and conditions of the Creative Commons Attribution (CC BY) license (<https://creativecommons.org/licenses/by/4.0/>).

1. Introduction

Since the invention of magnetic fluids in the 1960s, when this technology was developed by NASA for rocket fuels to transport them to the combustion chamber in a weightless state, they have moved on to being used in everyday devices [1]. Besides applications connected with dumping [2] and sealing [3], they are often used for heat transfer (dissipation) applications as well [4]. An example of this is a hard disk, where magnetic fluid is used as part of a magnetic head. Thanks to the magnetic properties of magnetic fluids, they can keep the magnetic head in the correct position while it moves over the magnetic disk. They also help cool the magnetic heads, which generate heat during data reading and writing, which has a positive impact on their power output. Another example of heat dissipation using magnetic fluid is a loudspeaker [4,5]. Its coil heats up due to its operation, while the magnetic fluid is kept in place by the magnetic field of a permanent magnet. Recently, there have been efforts to utilize the phenomenon of magnetoconvection for cooling transformers [6,7]. Technical equipment and its components may encounter heating even when subjected to high-frequency loads. If we want to apply magnetic fluids to these types of devices, we need to know their response to frequencies at the kilohertz level. We also need to understand how to regulate the thermal response to high-frequency magnetic fields. When a magnetic fluid containing superparamagnetic nanoparticles is exposed to a high-frequency alternating magnetic field, the particles undergo rapid changes

in magnetization direction. By applying an external magnetic field, the magnetic moments of the nanoparticles align in the direction of the field. When the field is turned off, the relaxation of the magnetic nanoparticles occurs in an equilibrium state via the Brownian or Néel relaxation mechanism, which is associated with the dissipation of energy into the surrounding particles [8–10]. The Brownian relaxation mechanism occurs when the entire particle rotates in the surrounding fluid with a typical relaxation time τ_B in the range of microseconds and can be expressed as follows:

$$\tau_B = 3V_H\eta/k_B T \quad (1)$$

where V_H is the hydrodynamic volume of the magnetic particle and η is the dynamic viscosity of the surrounding fluid; k_B —Boltzmann's constant ($1.38 \times 10^{-23} \text{ JK}^{-1}$), T —absolute temperature. The energy barrier for particle reorientation is determined by rotational friction in the surrounding fluid. Losses induced by the Brownian mechanism are also called viscous losses since heat generation is a consequence of viscous friction between the rotating particles and the surrounding medium. This type of loss is not limited to superparamagnetic particles. In general, particles that can be considered small permanent magnets with remanent magnetization M_R are subjected to a torque $T = \mu_0 M_R H V$ when exposed to a changing magnetic field H . In the equilibrium state, the viscous resistance in the fluid $12\pi\eta V f$ acts on the magnetic torque T , and the cycle's loss energy is given by $2\pi T$ [11]. The second mechanism is Néel relaxation [12], in which an external AC magnetic field provides energy that helps the magnetization vector to rotate inside the magnetic core of the particle and overcome the energy barrier $E = KV$, where K is the particle's anisotropy constant and V is the particle volume. The probability of this transition is $\exp(\sigma)$, where σ is the ratio of anisotropy energy to thermal energy $KV/k_B T$. The relaxation time τ_N of magnetic nanoparticles during Néel relaxation ranges from milliseconds (even several nanoseconds) to seconds and is given by the expression:

$$\tau_N = \tau_0 \cdot \exp(\sigma) = \tau_0 \cdot \exp(KV/k_B T) \quad (2)$$

where τ_0 is the damping or decay time (approximately 10^{-8} – 10^{-10} s). For high and low values of the energy barrier, we have:

$$\begin{aligned} \tau_N &= \tau_0 \cdot \sigma^{-1/2} \cdot \exp(\sigma), \sigma > 2 \\ &= \tau_0 \cdot \sigma, \sigma \ll 1. \end{aligned} \quad (3)$$

The particle size distribution causes the existence of a distribution of relaxation times, with both relaxation mechanisms contributing to magnetization. This creates the so-called effective relaxation time, where for specific particles:

$$\tau_{eff} = \tau_N \cdot \tau_B / (\tau_B + \tau_N) \quad (4)$$

The mechanism with the shortest relaxation time is dominant [9,12]. To quantify the magnetic heating ability of magnetic nanoparticles under the condition of an oscillating magnetic field, the "Specific Absorption Rate" (SAR) parameter is commonly used. SAR is defined as the amount of heating power (P , measured in watts) generated per unit mass of magnetic component in the sample (m_{MNP} in grams) [13]:

$$\text{SAR} = P/m_{MNP} \quad (5)$$

SAR depends on various factors, such as magnetic field intensity (H), frequency (f), concentration, magnetic permeability (μ), particle size and shape, the viscosity of the sample, and many other parameters, which are influenced either by the method of high-frequency magnetic field application or by the physical–chemical parameters of the investigated material [14,15]. In the work of Skumiel et al. [16], the heating characteristics of oil-based magnetic fluids of different magnetic particle concentrations were studied. The

samples with a lower volume fraction of magnetite exhibited a higher SAR value. Similar results were obtained when alternating [17] and rotating magnetic fields were applied [18]. In the latter cases, magnetite nanoparticles were suspended in an agar gel, and the thermal effect was clearly concentration-dependent. For samples with an agar concentration of 7%, the viscosity was approximately 100 mPa·s, several times higher than that for magnetic liquids. Despite such a high value for the viscosity coefficient in agar samples, the analysis of power losses of the thermal effect showed that there were losses resulting from both mechanisms (Néel and Brown). It was also found that with higher magnetite concentrations (smaller distances between NPs), the thermal effect determined according to Equation (5) became smaller. This can be explained by larger interactions between NPs. This can be attributed to the formation of aggregates in more concentrated magnetic fluids. Under maintaining consistent parameters, such as application conditions (H, f), as well as the type, size, and concentration of magnetic nanoparticles, viscosity plays a significant role. Indeed, this principle is at the core of the methodology, which aims to keep the samples and experimental parameters constant. In such conditions, the focus is on studying how viscosity, determined by various types of carrier liquid, influences the heat dissipation during an experiment in an applied high-frequency alternating magnetic field. If the magnetic particle size distribution in magnetic fluid is changing, it goes hand in hand with changes in rheological (viscosity) properties. It affects the magnetic moment of the particles, altering the strength of magnetic interactions and subsequently affecting the formation of aggregates in the magnetic fluid [19]. As was mentioned above, the magnetic relaxation processes can be strongly affected by viscosity. Numerous investigations have been carried out where authors tried to distinguish the contributions of Brownian and Néel relaxation to heating by varying the viscosity. To separate effects due to Néel or Brown relaxation, bacterial magnetic nanoparticles (magnetosomes) were immobilized by suspension in liquid gelatin [20]. Similar comparative SAR experiments were also conducted for magnetosome suspension and agar-based phantom samples [14]. The placement of magnetosomes in a gel structure led to a noticeable decrease in heating efficiency due to the limitation of Brownian motion. Cabrera et al. [21] analyzed the SAR values of iron oxide nanoparticles dispersed in water and agar. At low concentration ($3 \text{ mg}_{\text{Fe}} \cdot \text{mL}^{-1}$), SAR values measured in water and agar were comparable, but at the concentration of $10 \text{ mg}_{\text{Fe}} \cdot \text{mL}^{-1}$, SAR values in water were twice as high as in agar. The increase in SAR values in water at high particle concentration was associated with interparticle interaction effects that promote increased heat generation. In the present contribution, we analyzed the heating rate and SAR evolution of magnetic fluids prepared based on mineral oils with different viscosity. Understanding the influence of viscosity on heat dissipation in such types of fluids is important from the perspective of their use in conditions of oscillating magnetic fields in the technical science, as well as in the field of magnetic hyperthermia as a therapeutic tool in biomedicine, where fluids of different viscosities can serve as a model material for a deeper understanding of heat evolution under given conditions.

2. Experimental Materials and Methods

Magnetic Fluids (MF) Based on MOGUL, ITO 100, and MIDEL Oil

The magnetic fluids used were prepared based on the above-mentioned commercial mineral oils, MOGUL, ITO 100, and MIDEL, containing Fe_3O_4 magnetite nanoparticles coated with a surfactant—oleic acid. The preparation was carried out as follows: magnetite was synthesized by coprecipitation at around $80 \text{ }^\circ\text{C}$ using aqueous solutions of Fe^{3+} and Fe^{2+} ions along with a concentrated NH_4OH solution (25%). Surfactants were bound to the magnetic nanoparticles to provide steric stabilization (chemisorption of oleic acid at about $80 \text{ }^\circ\text{C}$). Magnetic decantation and multiple rinsing steps with acetone were used to remove byproducts of the precipitation reaction and obtain stabilized magnetic nanoparticles. The magnetic nanoparticles were then dispersed in a nonpolar liquid carrier at $120\text{--}130 \text{ }^\circ\text{C}$. Additional steps included magnetic decantation/filtration, flocculation, and redispersion of the magnetic nanoparticles to obtain a nonpolar magnetic fluid. To verify the binding

of oleic molecules to the surface of magnetic nanoparticles, Fourier-transform infrared spectroscopy (FTIR) was employed.

FTIR spectra were acquired using attenuated total reflectance (ATR) mode at room temperature within the wavelength range of $4000\text{--}500\text{ cm}^{-1}$, utilizing an FTIR spectrometer (ABB, Model FTLA2000-100, Québec, Canada). The spectral resolution was configured to 4 cm^{-1} .

Magnetization measurements were performed on the magnetic fluids based on mineral oils using a VSM magnetometer (MPMS-XL Quantum Design Inc., USA) at room temperature under a magnetic field of up to 5 T.

Hyperthermic parameters (specifically, the heating rate, dT/dt , and specific absorption rate, SAR) were obtained by measuring the T vs. t dependence in an alternating magnetic field (AMF). The LC circuit was powered by an alternating voltage generator with frequency f and voltage U . The coil induces a magnetic field, which causes a change in the magnetization of magnetic nanoparticles in the liquid, resulting in an increase in temperature. Measurements were performed at a frequency of 500 kHz in an alternating magnetic field with an amplitude of 0 to $5\text{ kA}\cdot\text{m}^{-1}$. Differential temperature measurements (of the magnetic fluid and a reference sample, i.e., oil as a liquid carrier) and isolation of the glass vial containing the sample from the coil winding by cooled flowing water were used to eliminate possible errors caused by parasitic heat contributions in the carrier liquid. The probes of the thermometer's optical fibers (FISO Technologies Inc., Québec, Canada) are not sensitive to the alternating magnetic field.

The rheological profile for the study of the flow properties of the samples was determined by using an MCR 502 rheometer (Anton Paar GmbH, Graz, Austria) in rotational mode. For all tests, the double-gap (DG) concentric cylinder arrangement was used with the characteristic volume of the sample 3.67 mL. The viscosity dependence of the samples on shear rate was recorded at $20\text{ }^{\circ}\text{C}$, with the shear rate varying within the range of 1 to 1000 1/s . The temperature dependence of the viscosity was measured in the temperature range from $25\text{ to }80\text{ }^{\circ}\text{C}$ at a constant shear rate of 50 1/s .

3. Particles, Oils, and Magnetic Fluid Parameters

Figure 1 illustrates the typical FTIR spectra of pure oleic acid (OA; depicted by the blue line), magnetic nanoparticles (Fe_3O_4 ; indicated by the black line), and magnetic nanoparticles coated with oleic acid ($\text{OA}@Fe_3O_4$; represented by the red line).

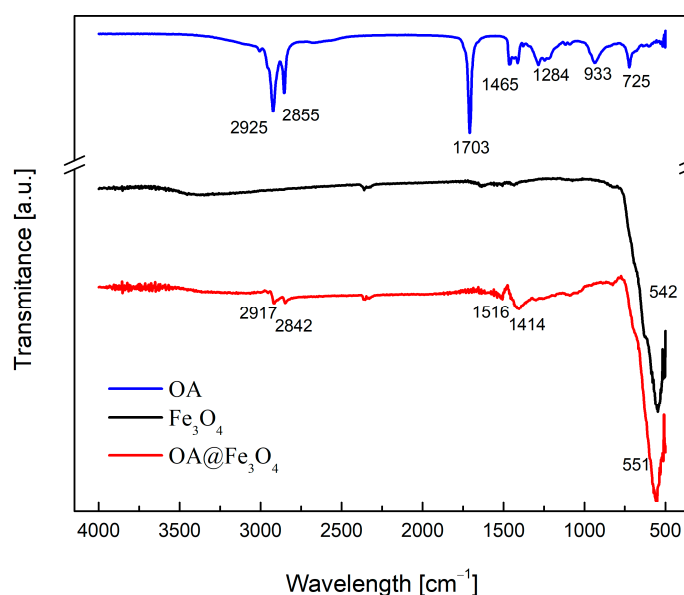


Figure 1. FTIR spectra of pure oleic acid (OA; blue), magnetic nanoparticles (Fe_3O_4 ; black), and coated magnetic nanoparticles using oleic acid ($\text{OA}@Fe_3O_4$; red).

For pure oleic acid, the peaks corresponding to the asymmetric CH_2 stretch and the symmetric CH_2 stretch vibrations appear at 2855 and 2925 cm^{-1} , respectively. The intense peak at 1710 cm^{-1} is attributed to the $\text{C}=\text{O}$ stretch, and the band at 1284 cm^{-1} signifies the presence of the $\text{C}-\text{O}$ stretch [22,23]. The peak at 542 cm^{-1} in the spectrum of magnetic nanoparticles is related to the $\text{Fe}-\text{O}$ group [24]. In the spectrum of $\text{OA}@Fe_3O_4$, when compared with the spectrum of pure OA, the $\nu_{\text{as}}(\text{CH}_2)$ and $\nu_{\text{s}}(\text{CH}_2)$ stretches shifted to 2842 and 2917 cm^{-1} , respectively. The band at 1710 cm^{-1} , corresponding to the stretching of $\text{C}=\text{O}$ in oleic acid, was absent in the spectrum of $\text{OA}@Fe_3O_4$. This can be explained by the absence of free surfactant in the sample. Instead, two new bands at 1414 and 1516 cm^{-1} appeared, attributed to the asymmetric and symmetric stretch vibration bands of the carboxylate group, respectively [25]. Moreover, the characteristic peaks of magnetic nanoparticles at 551 cm^{-1} are observed in the spectrum of $\text{OA}@Fe_3O_4$, confirming the presence of magnetic nanoparticles in the sample. These results show that the surface of magnetic particles was successfully coated with the surfactant.

The size distribution with a mean size of 12.2 nm of magnetite nanoparticles for each liquid carrier can be seen in Figure 2. Of course, since the same magnetic material was used, and prepared under the same conditions, the mean size is the same for all prepared magnetic fluids. The observed minimal differences may be related to the sample preparation methodology for the VSM experiment.

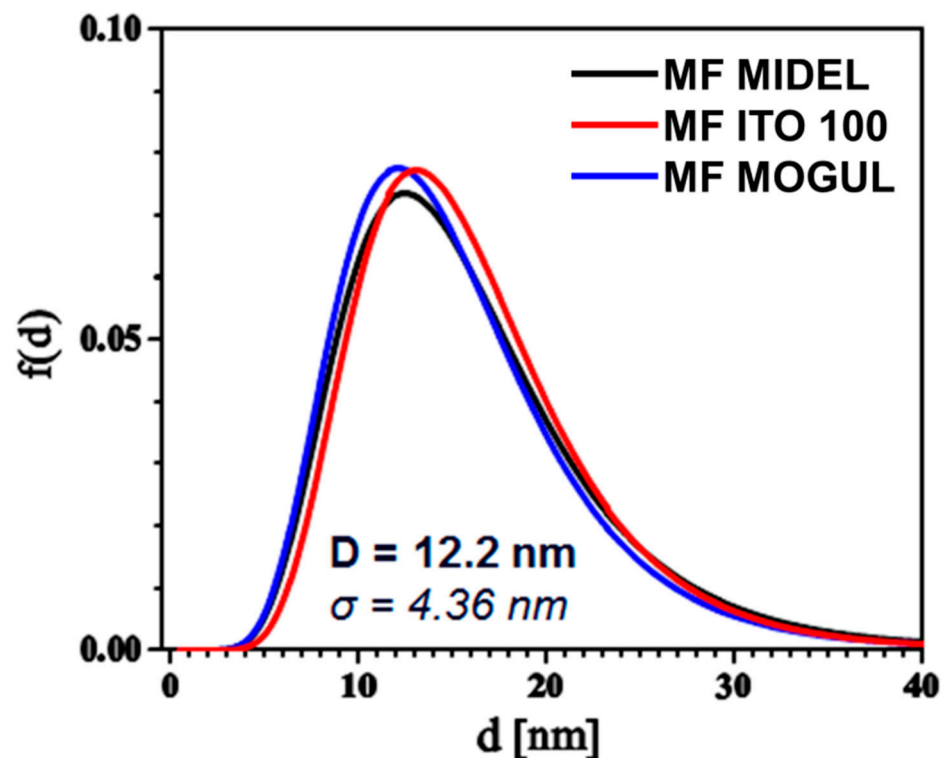


Figure 2. Lognormal distribution of magnetite particle sizes in the liquid carrier obtained from VSM data.

The magnetic core diameter of nanoparticles was calculated by fitting the initial magnetization curve to the Langevin model of magnetization in polydisperse ferrofluids. Details can be found in Raša [26]. The size distribution obtained from VSM analysis using Langevin fitting is not a direct measure of the physical size of particles obtained through imaging methods like TEM. Generally, for magnetic nanoparticles obtained via coprecipitation, the size distributions from magnetization measurements (magnetic core size) and TEM image analysis (physical size) do not differ significantly. Regarding the morphology of particles, they can be considered as roughly (quasi) spherical, as presented in the article by Kubovcikova et al. [27].

The obtained dependencies of magnetization on the applied magnetic field at room temperature are shown in Figure 3. From the measured dependencies, it can be seen that the samples did not exhibit hysteresis behavior and had approximately the same magnetization value. Of course, the obtained magnetic fluid saturation magnetization values ($\sim 26 \text{ emu}\cdot\text{g}^{-1}$) differed from those reported for their bulk counterparts ($92\text{--}100 \text{ emu}\cdot\text{g}^{-1}$) and usually decreased with size ($\sim 88 \text{ emu}\cdot\text{g}^{-1}$ for Fe_3O_4 nanoparticles) [28,29]. Another reason for the lower magnetic saturation is that uncoated magnetite nanoparticles in powder form constitute a different system compared to those in a magnetic fluid, due to particle coating, stability, and the presence of a carrier liquid. Moreover, particle concentration also plays a significant role, and it is necessary to realize that in magnetite converted into a magnetic fluid, the fraction of diamagnetic components increases, resulting in lower values. The basic parameters of the prepared mineral-oil-based magnetic fluids are listed in Table 1.

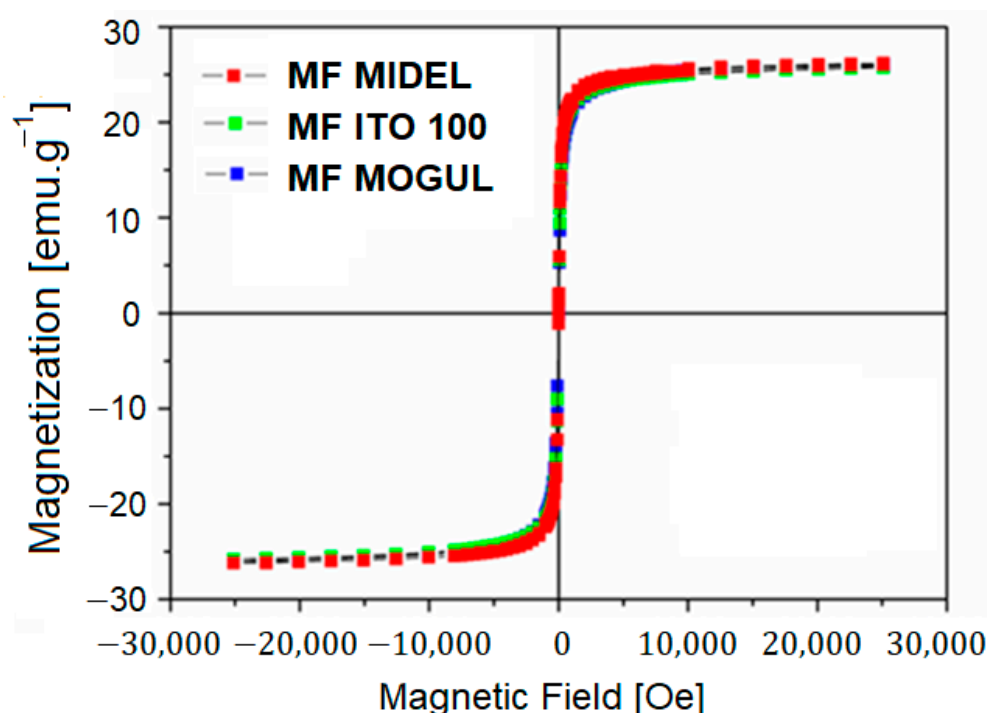


Figure 3. Dependency of magnetization on magnetic field at room temperature.

Table 1. Comparative characteristics of carrier liquids (mineral oils) vs. magnetic liquids prepared on them (ρ_{oil} —density of oils, ρ_{MF} —density of magnetic fluids, η_{oil} —viscosity of oils, η_{MF} —viscosity of magnetic fluids) and M_S -saturation magnetization values of magnetic fluids.

	$\rho_{\text{oil}} [\text{g}\cdot\text{cm}^{-3}]$	$\rho_{\text{MF}} [\text{g}\cdot\text{cm}^{-3}]$	$M_S [\text{emu}\cdot\text{g}^{-1}]$	$\eta_{\text{oil}} [\text{mPa}\cdot\text{s}]$	$\eta_{\text{MF}} [\text{mPa}\cdot\text{s}]$
MIDEL	0.975	1.202	26.10	55.48	85.51
ITO 100	0.895	1.128	25.70	16.28	52.30
MOGUL	0.791	1.031	25.90	12.51	44.54

For the purpose of evaluating the hyperthermic experiment, it was important to experimentally determine the viscosity characteristics of both mineral oils and the liquids prepared from these oils. This involved studying their behavior in relation to shear rate and examining the dependence of viscosity on temperature. In the entire range of measured shear rates, the oils under investigation exhibited an ideal viscous flow behavior, as demonstrated in Figure 4. The correlation between shear rate and dynamic viscosity reflects the characteristics of Newtonian fluids, where viscosity remains unaffected by shear rate.

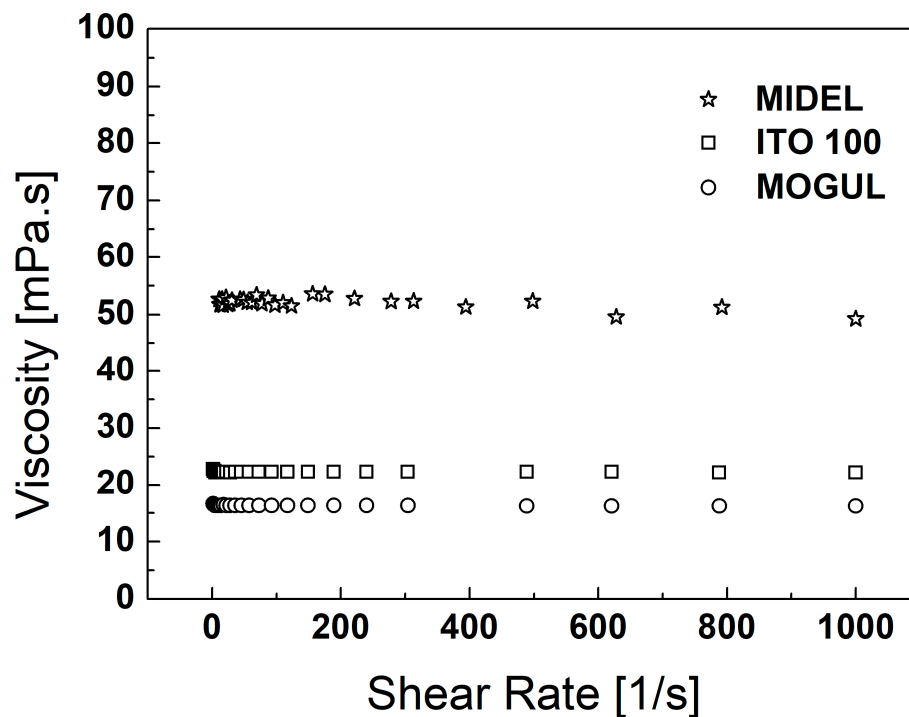


Figure 4. Dependency of viscosity on shear rate for various types of carrier liquids.

As previously demonstrated [30], the relationship between shear stress and shear rate for the oil-based magnetic fluid ITO 100 is linear, suggesting Newtonian fluid behavior. In our case (Figure 5), viscosity was also independent of shear rate, indicating that all magnetic fluids, prepared with various types of oils, exhibited Newtonian behavior as well. This observation indicates the stability of the magnetic fluids. The increased dynamic viscosity values in the case of magnetic fluids compared to bare oils correspond to the mass loading of the incorporated magnetic nanoparticles.

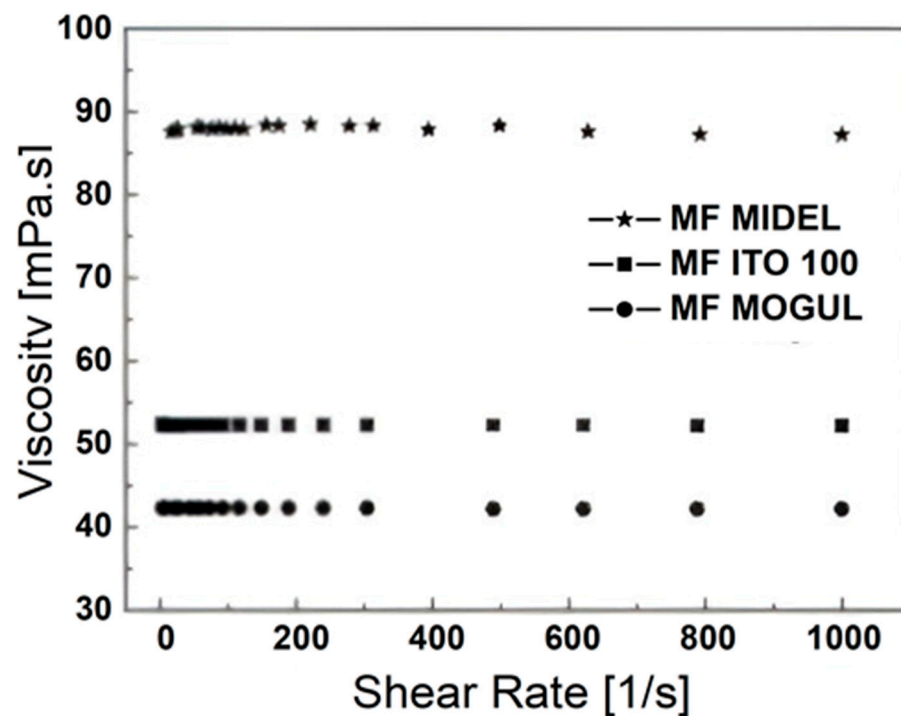


Figure 5. Dependency of viscosity of magnetic fluids on shear rate.

Understanding how viscosity changes with temperature is crucial for controlling the performance of the magnetic fluid in different conditions where thermal effects occur. The temperature dependences of viscosity (Figures 6 and 7) showed classical behavior, where an increase in temperature initiated a decrease in viscosity for all measured samples (oils and magnetic fluids). The initial viscosity at 25 °C was significantly higher in the case of magnetic fluids compared to the carrier fluids (mineral oils). For carrier oils ITO 100 and MOGUL, this increase in viscosity at 25 °C grew approximately 3.5 times after doping with particles—for MF ITO 100 and MF MOGUL. In the case of MIDEAL oil, viscosity increased by approximately 1.5 times. These differences in viscosity of the liquid carrier oil versus MF were roughly maintained across the entire temperature spectrum (up to the measured 80 °C). From this, we can conclude that the microstructure, or interactions between magnetic particles, did not play a role in the nature of the decrease in viscosity with increasing temperature. The decrease in both cases (carrier liquid and MF) was caused by the increased thermal energy within the liquid, leading to its movement and transition into a less organized state.

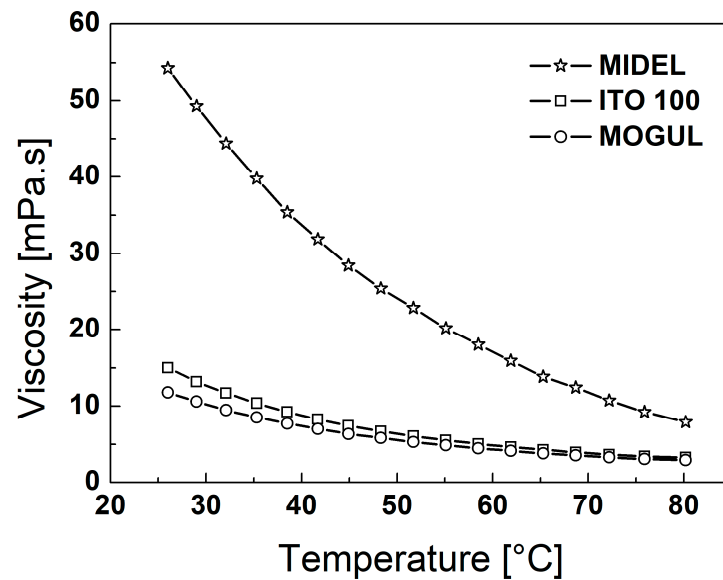


Figure 6. Dependency of viscosity of mineral oils (used as carrier liquids) on temperature.

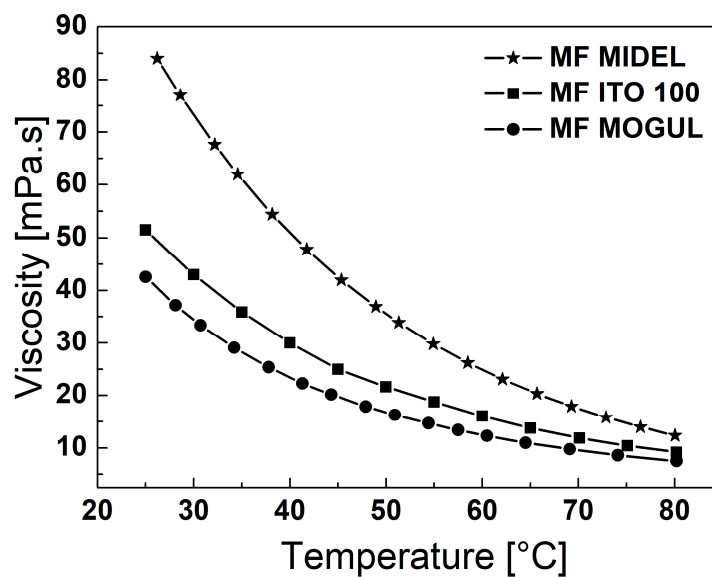


Figure 7. Temperature dependency of viscosity of magnetic liquids based on mineral oils.

These magnetic fluids represent a system of noninteracting magnetic nanoparticles that exhibit superparamagnetic behavior. This is also evidenced by the results obtained from saturation magnetization measurements, as we did not observe the existence of a hysteresis loop, and thus neither coercive field nor remanent magnetization. This fact is important for the evaluation of experiments obtained from hyperthermia, where dissipative losses and thus temperature increase originate only from relaxation losses and not from hysteresis losses.

4. Hyperthermal Properties of Magnetic Fluids

Experimental values of the heating rate $\Delta T/\Delta t$ as a function of the amplitude of the alternating magnetic field at 500 kHz were determined for magnetic fluids. The experimental data were fitted using the function $(H/a)^n$. The observed H^n -type dependence and the value of the power-law exponent “ n ”, which was the same for all samples with $n = 2$, provide information on the presence of superparamagnetic particles [10]. This fact is also supported by the size distribution, where individual magnetite particles can generally be considered superparamagnetic under these conditions [31]. Relaxation processes, namely Brownian and Néel relaxation, were responsible for generating energy losses. Indeed, the value of the exponent $n = 2$ of the power function $(H/a)^n$, as well as the course of the magnetization curve $M(H)$, clearly indicate the superparamagnetism of the samples and the lack of magnetic hysteresis. The following graph (Figure 8) shows the dependence of the temperature rise rate on the amplitude of the external magnetic field for magnetic fluids based on MOGUL, ITO 100, and MIDEL oil. The graph indicates that the coefficient of the temperature rise rate was indeed proportional to the square of the applied alternating magnetic field.

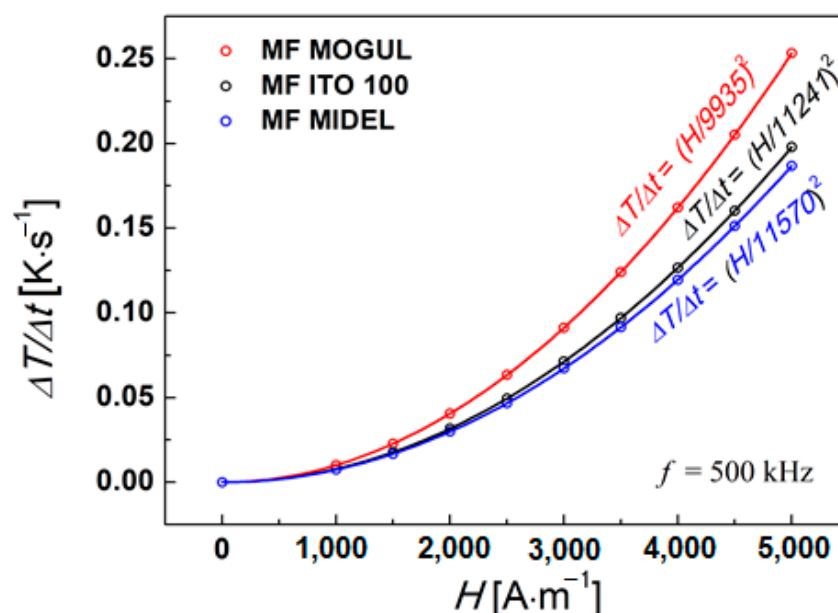


Figure 8. The rate of temperature increase $(\Delta T/\Delta t)_{t=0}$ as a function of the amplitude of the alternating magnetic field H at a frequency of $f = 500$ kHz for samples of mineral-oil-based magnetic fluids with varying viscosities.

Values of SAR of magnetic liquids are presented in Table 2, where the last column represents the conversion of SAR to grams of magnetic component, i.e., magnetite, per sample. As shown in Figure 9, at the same volume concentration of magnetic component (magnetite), viscosity of the liquid carrier played the most important role. Based on this, the SAR value increased with decreasing viscosity of the liquid carrier. This can be explained by the fact that particles in a medium with higher viscosity have a longer Brownian relaxation time and therefore contribute to energy losses to a lesser extent. In a liquid with higher

viscosity, such as MIDEL, the rotation of nanoparticles in the carrier liquid slows down, resulting in less friction and a smaller calorimetric effect, as illustrated in Figure 9.

Table 2. The SAR values obtained per gram of the sample and after conversion to the amount of magnetite in the sample.

Sample	Φ (Magnetic Volume Fraction) %	a (H/a) ²	SAR (Specific Absorption Rate) f = 500 kHz		
			5 kA·m ⁻¹	10 kA·m ⁻¹	10 kA·m ⁻¹
			W·g ⁻¹ _{sample}	W·g ⁻¹ _{sample}	W·g ⁻¹ _{Fe₃O₄}
MF MOGUL	6.6	9935	0.45	1.81	196.26
MF ITO 100	6.6	11,241	0.39	1.56	169.84
MF MIDEL	6.6	11,570	0.35	1.42	154.68

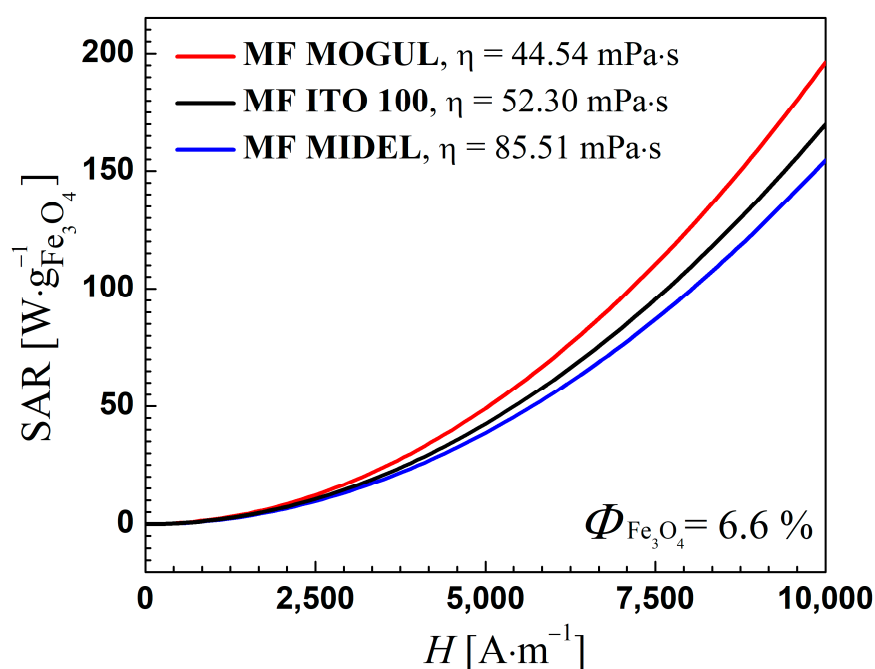


Figure 9. SAR depending on the intensity of the magnetic field at 500 kHz converted to the amount of magnetite in the sample. Magnetic fluids (MF) with liquid carriers MIDEL (154.68 W·g⁻¹), ITO 100 (169.84 W·g⁻¹), and MOGUL (196.26 W·g⁻¹). The stated MF SAR values were determined at 10 kA·m⁻¹.

5. Conclusions

This study focused on the preparation and evaluation of magnetic fluids under the application of a high-frequency oscillating magnetic field. The magnetic fluids were composed of magnetite nanoparticles coated with oleic acid surfactant and dispersed in commercially available mineral oils with varying viscosities. Viscosity plays a crucial role in magnetic hyperthermia as it directly impacts the efficiency of heat generation and distribution in the surrounding area. Understanding the properties of viscosity ensures uniform heat distribution and effective energy absorption, leading to improved heat dissipation control during oscillating magnetic field application. The experimental results obtained in this study align with the theoretical work of Raikher [32], who investigated the heating effects considering physical parameters such as the size and polydispersity of magnetic nanoparticles, magnetic parameters, crystal anisotropy, frequency, and viscosity of the carrier liquid. This research demonstrated that the absorption caused by the movement of

magnetic nanoparticles in the magnetic fluid significantly contributes to the specific absorption coefficient and, consequently, the specific power losses. The established relationship can describe both Néel and Brown relaxation mechanisms, allowing for the optimization of heating effects in the context of hyperthermia using single-domain magnetic nanoparticles.

Author Contributions: Conceptualization, M.M. and A.S.; methodology, M.M., A.S., J.T. and K.P.; formal analysis, M.M., M.T. and P.K.; investigation, M.M., A.S., J.T. and K.P.; resources, K.P.; data curation, M.M., A.S., J.T. and K.P.; writing—original draft preparation, M.M.; writing—review and editing, M.M., A.S., K.P., M.T. and P.K.; supervision, M.M.; funding acquisition, P.K. All authors have read and agreed to the published version of the manuscript.

Funding: This research was funded by the Slovak Academy of Sciences and the Ministry of Education, Slovakia, in the framework of projects VEGA 2/0011/20 and VEGA 1/0353/22, the Slovak Research and Development Agency under contracts No. APVV-22-0115 and APVV-22-0060, the project ITMS 313011T548 MODEX (Structural Funds of the EU, Ministry of Education, Slovakia), and the MVTs AZCAI (SAS-MOST JRP 2021/2) project.

Institutional Review Board Statement: Not applicable.

Informed Consent Statement: Not applicable.

Data Availability Statement: Data will be made available upon request.

Conflicts of Interest: The authors declare no conflict of interest.

References

1. Kole, M.; Khandekar, S. Engineering applications of ferrofluids: A review. *J. Magn. Magn. Mater.* **2021**, *537*, 168222. [\[CrossRef\]](#)
2. Yao, J.; Li, D.; Chen, X.; Huang, C.; Xu, D. Damping performance of a novel ferrofluid dynamic vibration absorber. *J. Fluids Struct.* **2019**, *90*, 190–204. [\[CrossRef\]](#)
3. Raj, K.; Moskowitz, B.; Casciari, R. Advances in ferrofluid technology. *J. Magn. Magn. Mater.* **1995**, *149*, 174–180. [\[CrossRef\]](#)
4. Scherer, C.; Figueiredo Neto, A.M. Ferrofluids: Properties and applications. *Braz. J. Phys.* **2005**, *35*, 718–727. [\[CrossRef\]](#)
5. Lee, M.Y.; Kim, H.J. Heat Transfer Characteristics of a Speaker Using Nano-Sized Ferrofluid. *Entropy* **2014**, *16*, 5891–5900. [\[CrossRef\]](#)
6. Patel, J.; Parekh, K.; Upadhyay, R.V. Prevention of hot spot temperature in a distribution transformer using magnetic fluid as a coolant. *Int. J. Therm. Sci.* **2016**, *103*, 35–40. [\[CrossRef\]](#)
7. Zanella, R.; Nore, C.; Bouillault, F.; Cappanera, L.; Tomas, I.; Mininger, X.; Guermont, J.L. Study of Magnetoconvection Impact on a Coil Cooling by Ferrofluid with a Spectral/Finite-Element Method. *IEEE Trans. Magn.* **2018**, *54*, 4600104. [\[CrossRef\]](#)
8. Philip, J. Magnetic nanofluids (Ferrofluids): Recent advances, applications, challenges, and future directions. *Adv. Colloid Interface Sci.* **2023**, *311*, 102810. [\[CrossRef\]](#)
9. Deatsch, A.E.; Evans, B.A. Heating efficiency in magnetic nanoparticle hyperthermia. *J. Magn. Magn. Mater.* **2014**, *354*, 163–172. [\[CrossRef\]](#)
10. Rosensweig, R.E. Heating magnetic fluid with alternating magnetic field. *J. Magn. Magn. Mater.* **2002**, *252*, 370–374. [\[CrossRef\]](#)
11. Hergt, R.; Dutz, S.; Uller, R.; Zeisberger, M. Magnetic particle hyperthermia: Nanoparticle magnetism and materials development for cancer therapy. *J. Phys. Condens. Matter.* **2006**, *18*, 2919–2934. [\[CrossRef\]](#)
12. Fannin, P.C. Magnetic spectroscopy as an aide in understanding magnetic fluids. *J. Magn. Magn. Mater.* **2002**, *252*, 59–64. [\[CrossRef\]](#)
13. Wildeboer, R.R.; Southern, P.; Pankhurst, Q.A. On the reliable measurement of specific absorption rates and intrinsic loss parameters in magnetic hyperthermia materials. *J. Phys. D Appl. Phys.* **2014**, *47*, 495003. [\[CrossRef\]](#)
14. Molcan, M.; Kaczmarek, K.; Kubovcikova, M.; Gojzewski, H.; Kovac, J.; Timko, M.; Józefczak, A. Magnetic hyperthermia study of magnetosome chain systems in tissue-mimicking phantom. *J. Mol. Liq.* **2020**, *320*, 114470. [\[CrossRef\]](#)
15. Garaio, E.; Sandre, O.; Collantes, J.M.; Garcia, J.A.; Mornet, S.; Plazaola, F. Specific absorption rate dependence on temperature in magnetic field hyperthermia measured by dynamic hysteresis losses (ac magnetometry). *Nanotechnology* **2015**, *26*, 015704. [\[CrossRef\]](#)
16. Skumiel, A.; Hornowski, T.; Józefczak, A. Heating characteristics of transformer oil-based magnetic fluids of different magnetic particle concentrations. *Int. J. Thermophys.* **2011**, *32*, 876–885. [\[CrossRef\]](#)
17. Skumiel, A.; Kaczmarek, K.; Flak, D.; Rajnak, M.; Antal, I.; Brząkała, H. The influence of magnetic nanoparticle concentration with dextran polymers in agar gel on heating efficiency in magnetic hyperthermia. *J. Mol. Liq.* **2020**, *304*, 112734. [\[CrossRef\]](#)
18. Musiał, J.; Skumiel, A.; Bielas, R. Study of the calorimetric effect in ferrogels subjected to the high-frequency rotating magnetic field. *J. Magn. Magn. Mater.* **2023**, *588*, 171462. [\[CrossRef\]](#)
19. Chen, S.; Li, D. Control of Magnetic Particle Size in Ferrofluid and Its Effect on Rheological Properties. *Chin. J. Mech. Eng. Engl. Ed.* **2022**, *35*, 79. [\[CrossRef\]](#)

20. Hergt, R.; Hiergeist, R.; Zeisberger, M.; Schüler, D.; Heyen, U.; Hilger, I.; Kaiser, W.A. Magnetic properties of bacterial magnetosomes as potential diagnostic and therapeutic tools. *J. Magn. Magn. Mater.* **2005**, *293*, 80–86. [[CrossRef](#)]
21. Cabrera, D.; Camarero, J.; Ortega, D.; Teran, F.J. Influence of the aggregation, concentration, and viscosity on the nanomagnetism of iron oxide nanoparticle colloids for magnetic hyperthermia. *J. Nanoparticle Res.* **2015**, *17*, 121. [[CrossRef](#)]
22. Ibarra, J.; Melendres, J.; Almada, M.; Burboa, M.G.; Taboada, P.; Juárez, J.; Valdez, M.A. Synthesis and characterization of magnetite/PLGA/chitosan nanoparticles. *Mater. Res. Express* **2015**, *2*, 095010. [[CrossRef](#)]
23. Zhang, L.; He, R.; Gu, H.C. Oleic acid coating on the monodisperse magnetite nanoparticles. *Appl. Surf. Sci.* **2006**, *253*, 2611–2617. [[CrossRef](#)]
24. Namduri, H.; Nasrazadani, S. Quantitative analysis of iron oxides using Fourier transform infrared spectrophotometry. *Corros. Sci.* **2008**, *50*, 2493–2497. [[CrossRef](#)]
25. Yang, K.; Peng, H.; Wen, Y.; Li, N. Re-examination of characteristic FTIR spectrum of secondary layer in bilayer oleic acid-coated Fe₃O₄ nanoparticles. *Appl. Surf. Sci.* **2010**, *256*, 3093–3097. [[CrossRef](#)]
26. Raşa, M. Magnetic properties and magneto-birefringence of magnetic fluids. *Eur. Phys. J. E* **2000**, *2*, 265–275. [[CrossRef](#)]
27. Kubovcikova, M.; Sobotova, R.; Zavisova, V.; Antal, I.; Khmara, I.; Lisnichuk, M.; Bednarikova, Z.; Jurikova, A.; Strbak, O.; Vojtova, J.; et al. N-Acetylcysteine-Loaded Magnetic Nanoparticles for Magnetic Resonance Imaging. *Int. J. Mol. Sci.* **2023**, *24*, 11414. [[CrossRef](#)]
28. Hadadian, Y.; Masoomi, H.; Dinari, A.; Ryu, C.; Hwang, S.; Kim, S.; Cho, B.K.; Lee, J.Y.; Yoon, J. From Low to High Saturation Magnetization in Magnetite Nanoparticles: The Crucial Role of the Molar Ratios between the Chemicals. *ACS Omega* **2022**, *7*, 15996–16012. [[CrossRef](#)]
29. Daoush, W.M. Co-Precipitation and Magnetic Properties of Magnetite Nanoparticles for Potential Biomedical Applications. *J. Nanomed. Res.* **2017**, *5*, 00118. [[CrossRef](#)]
30. Józefczak, A.; Hornowski, T.; Skumiel, A. Temperature dependence of particle size distribution in transformer oil-based ferrofluid. *Int. J. Thermophys.* **2011**, *32*, 795–806. [[CrossRef](#)]
31. Nguyen, M.D.; Tran, H.V.; Xu, S.; Lee, T.R. Fe₃O₄ Nanoparticles: Structures, Synthesis, Magnetic Properties, Surface Functionalization, and Emerging Applications. *Appl. Sci.* **2021**, *11*, 11301. [[CrossRef](#)] [[PubMed](#)]
32. Raikher, Y.L.; Stepanov, V.I. Physical aspects of magnetic hyperthermia: Low-frequency ac field absorption in a magnetic colloid. *J. Magn. Magn. Mater.* **2014**, *368*, 421–427. [[CrossRef](#)]

Disclaimer/Publisher’s Note: The statements, opinions and data contained in all publications are solely those of the individual author(s) and contributor(s) and not of MDPI and/or the editor(s). MDPI and/or the editor(s) disclaim responsibility for any injury to people or property resulting from any ideas, methods, instructions or products referred to in the content.